Research article

A Comparative Study on the Post-treatment Process of Sputtered SnO$_2$ Nanorod OAD Films

Thitiporn Kaewyou[1], Nampueng Pangpaiboon[1*], Tossaporn Lertvanithphol[2], Kata Jaruwongrungsee[2], Viyapol Patthanasettakul[2], Tawee Pogfay[2], Saksorn Limwichean[2] and Mati Horprathum[2]

[1]*Department of Industrial Physics and Medical Instrumentation, Faculty of Applied Science, King Mongkut's University of Technology North Bangkok, Bangkok, 10800, Thailand*
[2]*National Electronics and Computer Technology Center (NECTEC), National Science and Technology Development Agency, Pathum Thani, 12120 Thailand*

Abstract

The effects of single-step and two-step annealing and O$_2$ plasma treatments on SnO$_2$ slanted nanorods (SNR) films fabricated using DC magnetron sputtering and oblique angle deposition (OAD) was investigated in this study. The FE-SEM, AFM, and GI-XRD analyses demonstrate that both treatment approaches significantly influenced the film tilt angle, thickness, and surface morphology. After annealing, nanorod separation improved, surface roughness increased, and crystallinity was enhanced, particularly in the (110), (101), and (211) planes of the tetragonal rutile phase. In contrast, oxygen plasma treatments caused etching, reduced film thickness, and formed nano-necks at the tips of the slanted nanorods, leading to a reduction in crystallinity. Additionally, two-step treatments, particularly annealing followed by plasma treatment, achieved the best crystallinity while minimizing the etching effects of plasma. Finally, the optical properties, investigated using a UV–Vis–NIR spectrophotometer, demonstrated a progressive decrease in average transmittance within the visible region, from 86% to 79%, corresponding to the increasing number of post-treatment steps. In parallel, the optical bandgap was also found to decrease with additional treatments, shifting from 4.14 eV to 3.84 eV. The results highlight the importance of structural modifications in SnO$_2$ SNR films, as they directly influence film properties and enhance the potential for advanced optoelectronic device applications.

Keywords: SnO$_2$; slanted nanorod; OAD; DC magnetron sputtering; annealed treatment; O$_2$ plasma treatment

1. Introduction

SnO$_2$ nanostructure films have been widely studied due to their unique properties, such as high chemical stability, electrical conductivity, optical transparency, and wide bandgap ranging from 3.3 to 4.5 eV (Mun et al., 2015; Zakaria et al., 2022). These characteristics make them suitable for a variety of applications including gas sensors (Oros et al., 2016), transparent conductive oxides (TCOs), antibacterial coatings, photovoltaic cells, photocatalysis, lithium-ion batteries (LIBs), and catalysis, among others (Deka et al., 2020; Dalapati et al., 2021; Liu et al., 2022; Sun et al., 2022; Xavier et al., 2023; Patrun et al., 2024). The fabrication of SnO$_2$ nanostructures involves several techniques including sol-gel processing (Kumar et al., 2020), spray pyrolysis (Doubi et al., 2022), hydrothermal synthesis (Ihsan et al., 2025), electron beam evaporation (Lee et al., 2023), pulsed laser deposition (Hadi et al., 2024), and magnetron sputtering (Oros et al., 2016; Mykhailo et al., 2019). The magnetron sputtering technique with oblique angle deposition (OAD) has garnered significant attention due to its high deposition rate, excellent reproducibility, cost-effectiveness, and, most importantly, its scalability for industrial applications (Martin, 2009). This method enables precise control over nanostructure growth by adjusting the angle at which incoming particles strike the substrate, often approaching 80-89 degrees. As a result, the material is deposited at an angle, leading to the formation of slanted nanorods, where the nanorods tilt uniformly in the same direction (Angel et al., 2016). However, magnetron sputtering often results in low crystallinity due to its limited ionization effect (Limwichean et al., 2021).

Improving the crystallinity of films often involves post-treatments such as annealing and plasma treatment, each with distinct advantages and limitations. Annealing is widely employed to enhance crystallinity but require high temperatures, extended processing times, and poses risks of thermal stress (Orimi & Maghouli, 2016; Babu, et al., 2022). Plasma treatment, on the other hand, operates at lower temperatures with faster processing time and effectively modifies surface properties, though it may result in incomplete phase transitions compared to annealing (Chen et al., 2024). Recent studies have highlighted the potential of combining annealing and plasma treatment to improve film quality. For instance, Li et al. (2022) demonstrated that annealing TiO$_2$ fibers followed by H$_2$ plasma treatment generated oxygen vacancies, enhancing light absorption and reducing the bandgap. Similarly, Joshi et al. (2012) found that annealing colloidal ITO films at 150°C in air, followed by O$_2$ plasma treatment, significantly boosted their electrical properties. Additionally, Rasoo et al. (2020) explored the effects of Ar-plasma treatment combined with sulfur ambient annealing for the self-formation of indium nanostructures.

Studying the combined effects of annealing and plasma treatment on SnO$_2$ slanted nanorods (SNRs) remains underexplored. Such investigations could provide valuable insights for optimizing SNR properties, paving the way for improved performance in various applications. In this study, SnO$_2$ SNRs were synthesized using magnetron sputtering coupled with oblique angle deposition (OAD) techniques. The effects of single step annealing and O$_2$ plasma treatment were systematically examined. Furthermore, the two-step processes, which were annealing followed by plasma treatment and plasma treatment followed by annealing were explored to assess their combined impact. The physical, crystallographic, and optical properties of the SnO$_2$ SNRs were thoroughly analyzed to evaluate their potential for enhancing performance across various applications.

2. Materials and Methods

The SnO$_2$ SNR films were fabricated using DC magnetron sputtering with oblique angle deposition (OAD) on both Si and glass substrates. A 3-inch diameter tin (Sn) metal target of 99.99% purity (supplied by Kurt J. Lesker company) was utilized. Substrates were cleaned by sonication in isopropanol, acetone, and deionized water for 10 min each, followed by nitrogen drying, before being loaded into the deposition chamber. The sputtering was carried out under a gas mixture of Ar (99.99%) and O$_2$ (99.999%) at flow rates of 20 and 60 sccm, respectively, using a base pressure of 5×10^{-6} mbar and a working pressure of 3.0×10^{-3} mbar. The substrate was tilted at an angle of 85 degrees relative to the vapor flux, as illustrated in the schematic diagram in Figure 1. During the deposition process, the substrate remained stationary and unheated, with DC power set to 150 W for a duration of 90 min. After deposition, the As-deposited SnO$_2$ SNR films were subjected to four different treatment methods to modify the film structure. The single-step treatments included: 1) Annealing in ambient air at 400°C for 2 h, with a heating rate of 10°C per min. Following this annealing period, the temperature was gradually lowered to room temperature (Anneal). 2) Oxygen plasma treatment using an RF generator in sputtering systems, where the pressure was set at 1×10^{-2} mbar and the RF power was maintained at 50W for 10 min (O$_2$-Plasma). The two-step treatments consisted of: 3) Annealing followed by oxygen plasma treatment (Anneal/O$_2$-Plasma) and 4) Oxygen plasma treatment followed by annealing (O$_2$-Plasma/Anneal).

The physical morphology of all prepared SnO$_2$ SNR films was analyzed using a field-emission scanning electron microscopy (FE-SEM; Hitachi High Tech. SU8030) and atomic force microscopy (AFM; HITACHI AFM 5300E) with a scan area of 1×1 µm². The crystal structure was examined by grazing incidence X-ray diffraction (GIXRD, Rigaku) with monochromatized Cu Kα radiation at 50 kV and 300 mA. The XRD measurements were conducted in 0.02° steps, scanning from 20° to 70° at a speed of 3°/min. Optical properties, including total average transmittance and optical band gaps, were assessed using a UV–Vis–NIR spectrophotometer (Agilent Cary 7000 with universal measurement accessory) over a wavelength range of 250-1750 nm.
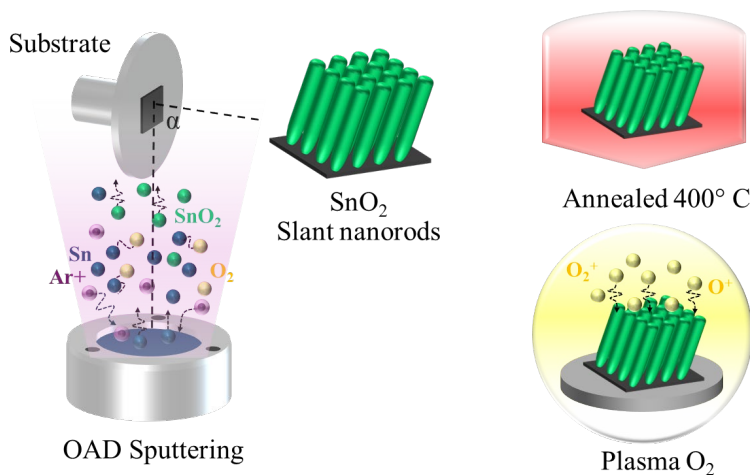

Figure 1. Schematic diagram of preparation of crystalline SnO$_2$ SNRs by annealing process in comparison with O$_2$ plasma treatment

3. Results and Discussion

Figure 2 presents a cross-sectional image illustrating the structural characteristics of the entire film. The prepared film exhibited a slanted nanorod structure with a length of 721 nm and an inclination angle of 22° relative to the silicon substrate, as shown in Figure 2(a). The annealing and plasma treatments showed that the slanted nanorods largely retained their shape, with a slight increase in tilt angle, where the annealing process caused a greater increase in tilt angle compared to the plasma treatment, as shown in Figure 2(b). Regarding thickness, plasma treatment led to a greater reduction in film thickness compared to annealing. This reduction was due to etching or resputtering caused by oxygen ion bombardment on the nanorod surface, which resulted in decreased film thickness, which was consistent with previous research (Zhang et al., 2010; Xie et al., 2017; Hasani, 2022). When the film was annealed prior to plasma treatment, a slight reduction in the thickness of the slanted nanorod film was observed. This was attributed to the annealing process, which helped restructure the film's orientation, reduce porosity, and improve packing density (Limwichean et al., 2021). These changes subsequently led to less etching during plasma treatment.
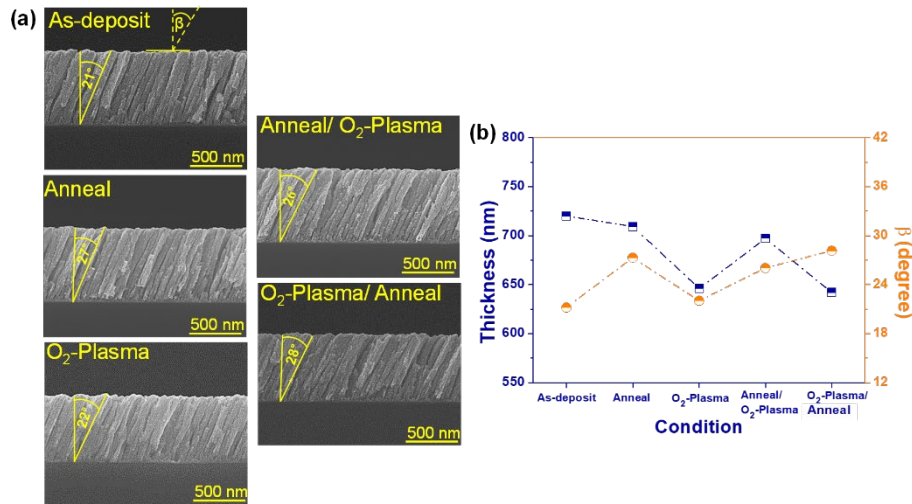

Figure 2. (a) Cross-section (SEM) images and angle, (b) Thickness of SnO_2 SNRs prepared at different processes are As-deposit, Anneal, O_2-Plasma, Anneal/O_2-Plasma, and O_2-Plasma/Anneal

Figure 3 displays SEM images illustrating the surface characteristics of the films. Following modifications to the surface, the films exhibit marked changes. The process of annealing leads to greater spacing among the slanted nanorod structures as increased temperatures boost atomic mobility. This elevated mobility facilitates continuous atomic diffusion, which enhances the alignment of the nanorods (Xie et al., 2017). Conversely, plasma treatment with oxygen ions induces surface bombardment, contributing to the development of nano-necks at the tips of the nanorods. The analysis of % porosity, based on the void area between nanorods using surface images processed with the Image-J program, showed that after annealing, the porosity reached a peak of 38.55%, indicating

increased separation of the nanorods. In contrast, the plasma-treated film exhibited the lowest porosity at 26.48%, suggesting greater interconnection between the nanorods. In the two-step surface treatments, annealing before plasma treatment also resulted in the formation of nano-necks, though to a lesser extent than in the single-step plasma treatment, as reflected by the smaller reduction in porosity. For the plasma-treated films, the annealing process caused a slight increase in structural separation. These findings highlight the significant impact of surface modifications on tilted nanorods, leading to either clear separation of nanorods or the development of nano-necks between adjacent grains. The efficacy of single-step treatments (annealing or O_2-plasma only) was evident in their suitability for applications demanding a high surface-to-volume ratio, such as gas sensors and photocatalysts. However, two-step treatments (Anneal/O_2-Plasma or O_2-Plasma/Anneal) offered a distinct advantage by improving electrical conductivity, which is attributed to facilitated electron transfer across the Schottky barrier in sensor devices (Moon et al., 2013; Song et al., 2017).
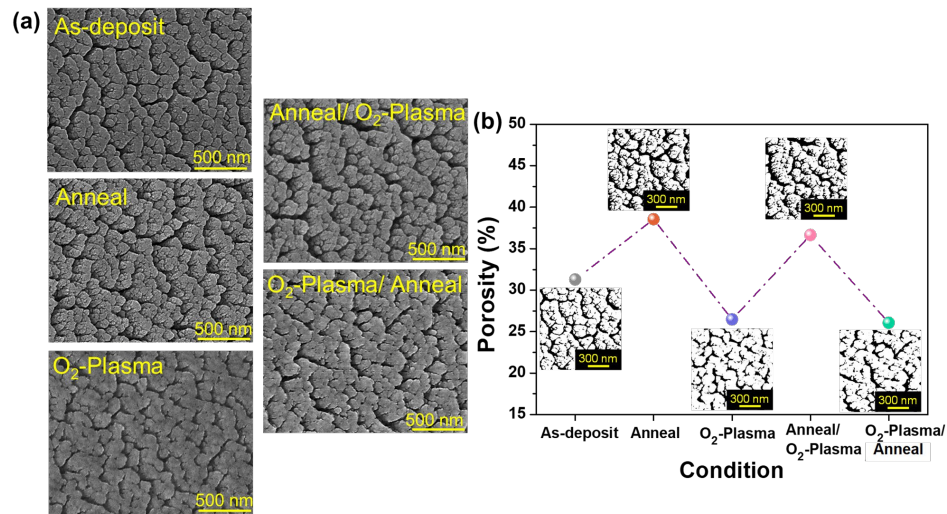

Figure 3. (a) Surface (SEM) image, (b) Porosity percentage of SnO_2 SNRs prepared at different processes: As-deposit, Anneal, O_2-Plasma, Anneal/O_2-Plasma, and O_2-Plasma/Anneal

       The surface roughness of SnO_2 SNRs was evaluated using root mean square (RMS) analysis, which indicated that RMS values increased after both single-step and two-step surface modifications, as shown in Figure 4. This is common behavior in thin film structures when exposed to surface modification by heating, as the increased energy enhances atomic mobility, causing rearrangement and grain growth. These microstructural changes lead to a rougher surface (Tao et al., 2020; Dangi et al., 2023). The highest surface roughness was achieved through a combination of annealing and plasma treatment, resulting in an RMS value of 14.71 nm. Further analysis revealed that annealing had a greater effect on roughness than plasma treatment, due to its longer duration and higher accumulated temperature, which allowed heat to diffuse throughout the structure. Additionally, the creation of voids between the nanorods further contributed to the increased roughness.
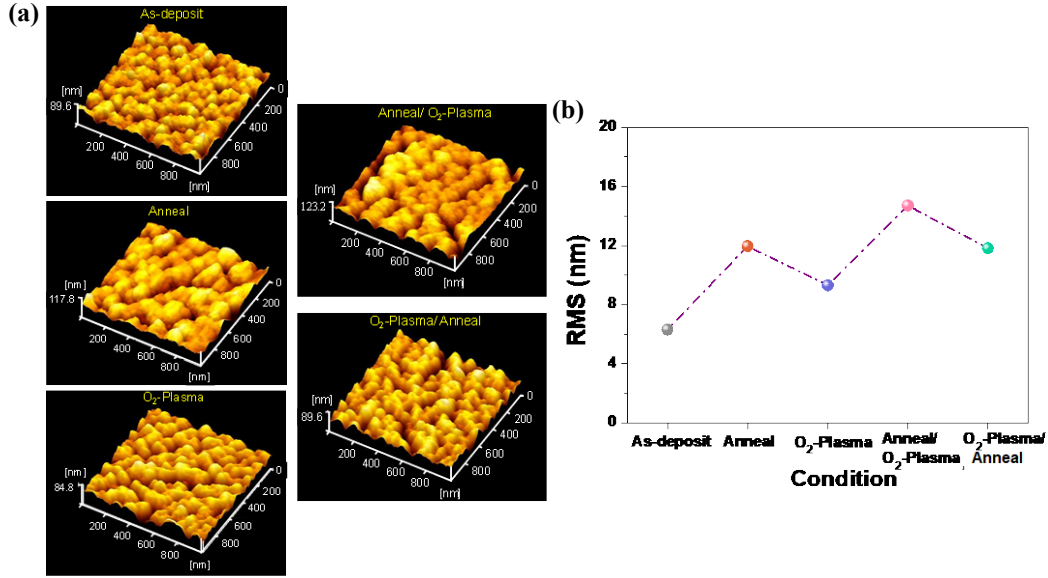
Figure 4. (a) The typical AFM images and (b) RMS roughness of the SnO$_2$ SNRs prepared at different processes: As-deposit, Anneal, O$_2$-Plasma, Anneal/O$_2$-Plasma, and O$_2$-Plasma/Anneal

The structure of the SnO$_2$ nanorods (NR) was investigated using GI-XRD. Analysis of five samples indicated that all films exhibited phases corresponding to the (110), (101), and (211) planes of the tetragonal rutile phase (JCPDS # 041-01445), with differences in peak intensities (Oros et al., 2016). It was observed that the crystallinity of the film increased after annealing, which is typical behavior for thin films. In contrast, single-step oxygen plasma treatment reduces crystallinity. However, films that underwent annealing prior to plasma treatment showed improved crystallinity. These results emphasize the significance of the packing density of SnO$_2$ NR films in enhancing crystallinity through plasma treatment. Additionally, the average crystallite size was determined from all diffraction peaks using Scherrer's formula (Ihsan et al., 2025).

$$D = \frac{K\lambda}{\beta cos\theta} \tag{1}$$

According to equation (1), D represents the crystallite size, K is the shape factor (commonly taken as 0.9 for spherical particles), λ is the X-ray wavelength of the Cu Kα$_1$ radiation (1.54059 Å), B is the full width at half maximum (FWHM) in radians, and θ is the Bragg diffraction angle in degrees. The FWHM values used in this study were obtained via Gaussian fitting of the corresponding diffraction peaks. These values were then applied in equation (1) to estimate the crystallite sizes for specific Bragg reflection planes, as crystallite size depends on the orientation of the lattice planes. The experimental results clearly demonstrate that annealing increases the crystallite size, while plasma treatment reduces it, as shown in Table 1. However, when annealing is followed by plasma treatment, the crystallite size reaches its maximum, indicating this combined approach enhances crystal growth most effectively.
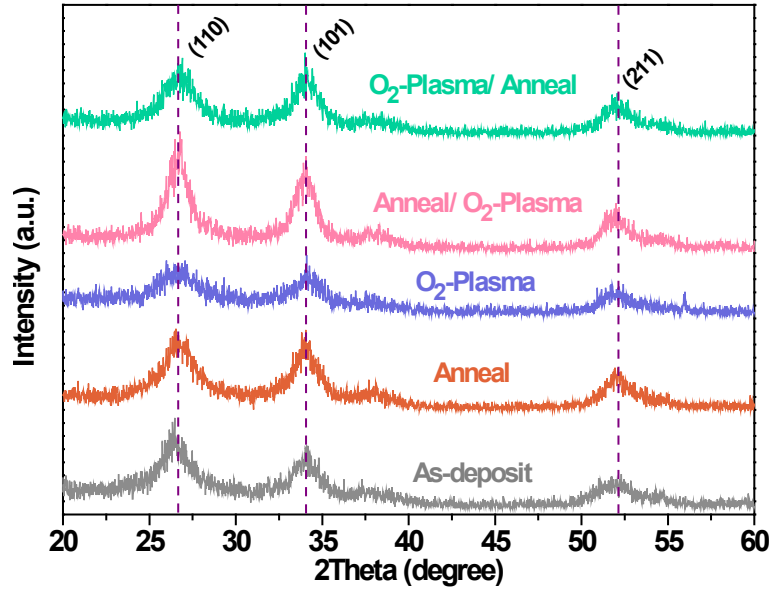
Figure 5. XRD diffraction pattern of the SnO₂ SNRs prepared at different processes: As-deposit, Anneal, O₂-Plasma, Anneal/O₂-Plasma, and O₂-Plasma/Anneal

Table 1. The crystalline sizes of SnO₂ SNR films as determined from X-ray diffraction data using Gaussian fitting calculations.

Condition	XRD Peak 2Θ (°)			d (Å)			FWHM		
	(110)	(101)	(211)	(110)	(101)	(211)	(110)	(101)	(211)
As-deposit	26.48	34.06	51.97	0.6139	0.7398	0.4912	2.32	1.96	3.14
Anneal	26.72	34.03	52.17	0.5864	0.7552	0.6101	2.43	1.92	2.53
Plasma	26.71	34.13	52.14	0.4703	0.5143	0.5572	3.03	2.82	2.77
Anneal/ O₂-Plasma	26.68	34.01	52.11	0.8332	0.8787	0.6051	1.71	1.65	2.55
O₂-Plasma/ Anneal	26.73	34.06	52.14	0.5891	0.7513	0.5891	2.42	1.93	2.62

The optical properties of SnO₂ SNRs were examined by measuring the transmission spectra of the prepared samples on glass slide substrates. These measurements, performed in the range of 300-1800 nm at normal incidence using a UV–Vis–NIR spectrophotometer, are displayed in Figure. 6. The results showed that all treatment samples had an impact on optical interference, film transparency, and absorption coefficient. For comparison purposes, the average transmittance (T_{Avg}) of the samples was determined by calculating the integral visible transmittance within the 380-780 nm range using the following equation (Limwichean et al., 2021).

$$T_{Avg} = \frac{\int \phi_{lum}(\lambda)T(\lambda)d(\lambda)}{\int \phi_{lum}(\lambda)d(\lambda)} \quad (2)$$

where T(λ) represents the transmittance at a specific wavelength (λ) within the visible spectrum, and ϕ_{lum} is the standard luminous efficiency function, corresponding to the human eye's sensitivity to light.

The T_{Avg} values for the SnO$_2$ SNRs were calculated as follows: 89.55% for the As-deposited sample, 84.05% for the annealed sample, 86.38% for the plasma-treated sample, 80.70% for the annealed-plasma sample, and 78.55% for the plasma-annealing sample, as shown in Figure 6(b). The results indicate that after surface modification, the average transmittance (T_{Avg}) decreased. This reduction was attributed to the increased surface roughness, which enhanced both light scattering and reflection (Tao et al., 2020). Additionally, it can be observed that the increased tilt angle correlated with the decrease in T_{Avg}. Therefore, it could be suggested that the greater tilt angle also contributed to light scattering and reflection, a point that warrants further investigation. Finally, the transmittance spectra can be converted into the absorption coefficient to evaluate the band gap energy. The absorption coefficient was calculated based on the method outlined by Velevska et al. (2017).

$$\alpha(v) = \frac{1}{d} ln \frac{1}{T} \tag{3}$$

where T denotes the transmittance spectra measured and *d* is the thickness of the film.

The band gap energy was determined by extrapolating the linear region of the Tauc plot using Tauc's equation (Velevska et al., 2017).

$$(\alpha h v)^2 = A(h v - E_g) \tag{4}$$

where *A* is a constant, *hv* represents the incident photon energy, E_g is the band gap energy, and *α* is the absorption coefficient. The index *n* defines the type of electronic transitions responsible for absorption.

Figure 6(c) shows the calculated energy gaps of the SnO$_2$ SNR films for the As-deposited, Annealed, O$_2$-Plasma, Anneal/O$_2$-Plasma, and O$_2$-Plasma/Anneal samples, recorded as approximately 4.14, 3.97, 4.10, 3.85, and 3.84 eV, respectively. These results indicate that post-treated SnO$_2$ SNR films exhibited enhanced absorption of lower-energy photons, leading to a reduction in optical transmittance, which was consistent with observations from previous studies (Orimi & Maghouli, 2016; Pan et al., 2019). Furthermore, the findings reflect the wide optical band gap of SnO$_2$ films reported in the literature, which ranges from 3.3 to 4.5 eV (Mun et al., 2015; Zakaria et al., 2022). In one-step surface modification, annealing has a more pronounced effect on the optical band gap than O$_2$ plasma treatment. This is due to annealing improving the crystalline structure more effectively and reducing defects in the film, resulting in more stable nanostructures. Additionally, in two-step surface modification, the energy gap reductions are similar, regardless of whether plasma treatment or annealing is applied first, suggesting that the order of the processes does not significantly impact the change in the band gap energy. The overall analysis highlights the importance of this study, demonstrating the differences between annealing and plasma treatments, as well as two-step surface modifications and their effects on SnO$_2$ SNRs. These treatments impact the physical characteristics, crystallinity of thin films, and optical properties. The insights gained from this study can be further applied to enhance the performance of optoelectronic devices.
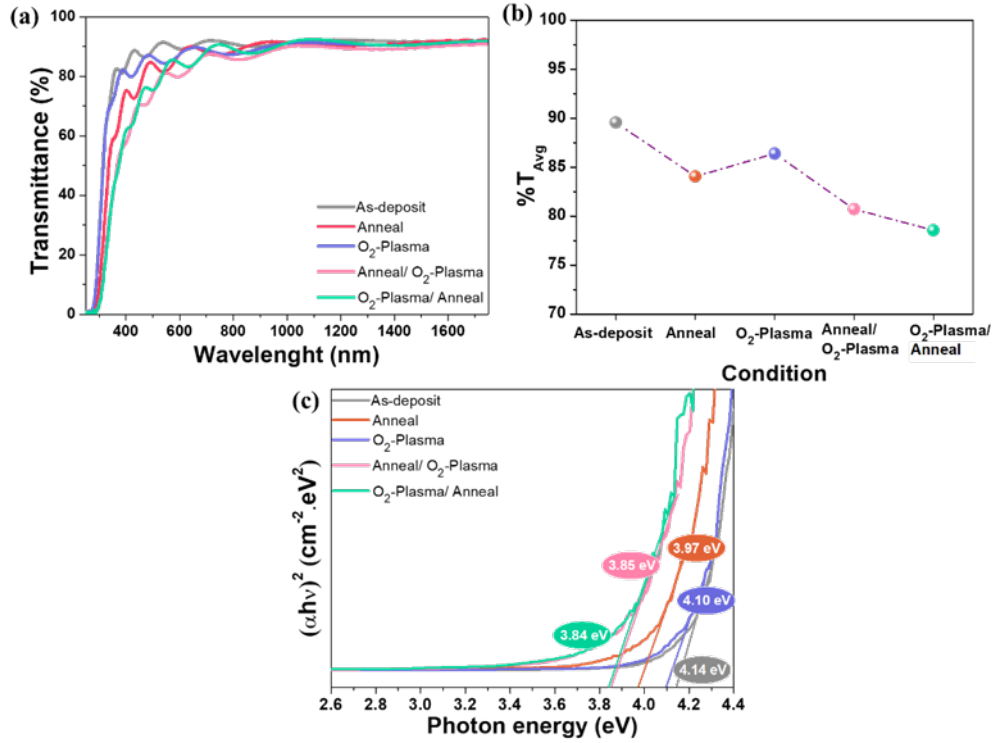
Figure 6. (a) The transmittance spectra, (b) the average transmittance in visible light range, and (c) Tauc's optical band gap plot of the SnO_2 SNRs prepared at different processes: As-deposit, Anneal, O_2-Plasma, Anneal/O_2-Plasma, and O_2-Plasma/Anneal

4. Conclusions

In this study, we investigated the impact of annealing and oxygen plasma treatment on SnO_2 slanted nanorod (SNR) films prepared through DC magnetron sputtering with oblique angle deposition (OAD). The findings show that both single-step and two-step treatments significantly affected the characteristics of the SnO_2 SNR films. Annealing improved the separation between the slanted nanorods, resulting in better alignment and enhanced morphology. In contrast, O_2 plasma treatment which involved ion bombardment, reduced the film thickness and promoted the formation of nano-necks at the tips of the nanorods. In the two-step process, annealing before O_2 plasma treatment played a crucial role in minimizing the etching effects and preserving the structural integrity of the nanorods. Additionally, this combination resulted in the highest crystallinity, although single-step O_2 plasma treatment led to a reduction in crystallinity. In terms of optical properties, all surface modifications resulted in a slight decrease in transparency. The single-step O_2 plasma treatment exhibited the highest transparency, with an average transmission (T_{Avg}) of 86%. Moreover, the treatments caused a reduction in the optical bandgap, which enhanced film stability. These results highlight the effectiveness of post-treatments in enhancing the properties of SnO_2 SNR films, making them more suitable for optoelectronic applications. Furthermore, all processes can be carried out within a single magnetron sputtering system, facilitating scalability for commercial production.

5. Acknowledgements

6. Conflicts of Interest

The authors have declared that they have no conflicts of interest.

ORCID

Nampueng Pangpaiboon https://orcid.org/0000-0002-2190-9892

Tossaporn Lertvanithphol https://orcid.org/0009-0009-1334-6944

Kata Jaruwongrungsee https://orcid.org/0000-0003-0724-5804

Tawee Pogfay https://orcid.org/0000-0003-0335-1335

Saksorn Limwichean https://orcid.org/0000-0001-6899-7853

Mati Horprathum https://orcid.org/0000-0003-1507-3555

References

Angel, B., Ana, B., Agustin, R. G-E., & Alberto, P. (2016). Perspectives on oblique angle deposition of thin films: From fundamentals to devices. *Materials Chemistry and Physics*, 76, 59-153. https://doi.org/10.1016/j.pmatsci.2015.06.003

Babu, B., Talluri, B., Gurugubelli, T. R., Kim, J., & Yoo, K. (2022). Effect of annealing environment on the photoelectrochemical water oxidation and electrochemical supercapacitor performance of SnO_2 quantum dots. *Chemosphere*, 286(Part 1), Article 131577. https://doi.org/10.1016/j.chemosphere.2021.131577

Chen, F., Chen, G., Huang, J., Chen, W., Guo, Y., Ma, J., Zhao, Z., Li, T., & Ostrikov, K. (Ken). (2024). Plasma-surface-modified SnO_2–CuCl nanocomposite for highly selective electrocatalytic CO_2 conversion. *Ceramics International*, 50(5), 8439-8447. https://doi.org/10.1016/j.ceramint.2023.12.179

Dalapati, G. K., Sharma, H., Guchhait, A., Chakrabarty, N., Bamola, P., Liu, Q., Saianand, G., Krishna, A. M. S., Mukhopadhyay, S., Dey, A., Wong, T. K. S., Zhuk, S., Ghosh, S., Chakrabortty, S., Mahata, C., Biring, S., Kumar, A., Ribeiro, C. S., Ramakrishna, S., Chakraborty, A. K., Krishnamurthy, S.,…Sharma, M. (2021). Tin oxide for optoelectronic, photovoltaic and energy storage devices: A review. *Journal of Materials Chemistry A,* 9(31), 16621-16684. https://doi.org/10.1039/d1ta01291f

Dangi, R., Basnet, B., Pandey, M., Bhusal, S., Budhathoki, B., Parajuli, K., Tiwari, S. K., & Kafle, B. P. (2023). Effect of oxygen vacancy on the crystallinity and optical band gap in tin oxide thin film. *Energies*, 16(6), Article 2653. https://doi.org/10.3390/en16062653

Deka, R. C., Deka, A., Deka, P., Saikia, S., Baruah, J., & Sarma, P. J. (2020). Recent advances in nanoarchitectonics of SnO_2 clusters and their applications in catalysis.

Journal of Nanoscience and Nanotechnology, 20(8), 5153-5161. https://doi.org/10.1166/jnn.2020.18539

Doubi, Y., Hartiti, B., Siadat, M., Ziti, A., Stitou, M., Nkuissi, H. J. T., Labrim, H., Fadili, S., Tahri, M., Thevenin, P., & Losson, E. (2022). Theoretical validation of the properties of SnO_2 nanostructure grown by robust spray pyrolysis technique for formaldehyde gas sensor. *Materials Today: Proceedings*, 66(Part 1), 341-345. https://doi.org/10.1016/j.matpr.2022.05.440

Hadi, A. J., Nayef, U. M., Mutlak, F. A.-H., & Jabir, M. S. (2024). Enhancing photodetection performance through laser fluence control: SnO_2 nanostructured deposited on porous silicon. *Optics and Laser Technology*, 179, Article 111338. https://doi.org/10.1016/j.optlastec.2024.111338

Hasani, E. (2022). Effect of treatment time and radio frequency power on roughness and wettability of oxygen plasma-etched cadmium telluride thin films. *Thin Solid Films,* 761, Article 139499. https://doi.org/10.1016/j.tsf.2022.139499

Ihsan, S., Zulfiqar, S., Khattak, S. A., Albargi, H. B., Khan, A., Rooh, G., Khan, T., Khan, G., & Ullah, I. (2025). The effect of solvent on the structural, morphological, optical and dielectric properties of SnO_2 nanostructures. *Physica E: Low-Dimensional Systems and Nanostructures*, 165, Article 116095. https://doi.org/10.1016/j.physe.2024.116095

Joshi, S. M., Book, G. W., & Gerhardt, R. A. (2012). A comparative study of the effect of annealing and plasma treatments on the microstructure and properties of colloidal indium tin oxide films and cold-sputtered indium tin oxide films. *Thin Solid Films*, 520(7), 2723-2730. https://doi.org/10.1016/j.tsf.2011.11.052

Kumar, P., Khadtare, S., Park, J., & Yadav, B. C. (2020). Fabrication of leaf shaped SnO_2 nanoparticles via sol–gel route and its application for the optoelectronic humidity sensor. *Materials Letters*, 278, 128451. https://doi.org/10.1016/j.matlet.2020.128451

Lee, J., Min, H., Choe, Y.-S., Lee, Y. G., Kim, K., Lee, H.-S., & Lee, W. (2023). Highly sensitive and selective detection of benzene, toluene, xylene, and formaldehyde using Au-coated SnO_2 nanorod arrays for indoor air quality monitoring. *Sensors and Actuators B: Chemical*, 394. Article 134359. https://doi.org/10.1016/j.snb.2023.134359

Li, D., Xu, K., Zhenyu, N., & Zhang, C. (2022). Annealing and plasma effects on the structural and photocatalytic properties of TiO_2 fibers produced by electrospinning. *Catalysts*, 12(11), Article 1441. https://doi.org/10.3390/catal12111441

Limwichean, S., Eiamchai, P., Ponchio, C., Kasayapanand, N., & Horprathum, M. (2021). Comparative investigations of DCMS/HiPIMS reactively sputtered WO_3 thin films for photo-electrochemical efficiency enhancements. *Vacuum*, 185, Article 109978. https://doi.org/10.1016/j.vacuum.2020.109978

Liu, D., Zheng, H., Ahmed, Y., Zheng, C., Wang, Y., Chen, H., Chen, L., & Li, S. (2022). Enhanced photovoltaic performance of SnO_2 based flexible perovskite solar cells via introducing interfacial dipolar layer and defect passivation. *Journal of Power Sources*, 519, Article 230814. https://doi.org/10.1016/j.jpowsour.2021.230814

Martin, P. M. (2009). *Handbook of deposition technologies for films and coatings*. (3rd ed.). Elsevier.

Moon, H. G., Choi, Y. R., Shim, Y.-S., Choi, K.-I., Lee, J.-H., Kim, J.-S., Yoon, S.-J., Park, H.-H., Kang, C.-Y., & Jang, H. W. (2013). Extremely sensitive and selective NO probe based on villi-like WO_3 nanostructures for application to exhaled breath analyzers. *ACS Applied Materials and Interfaces*, 5(21), 10591-10596. https://doi.org/10.1021/am402456s

Mun, H., Yang, H., Park, J., Ju, C., & Char, K. (2015). High electron mobility in epitaxial SnO_{2-x} in semiconducting regime. *APL Materials*, 3(7), 076107. https://doi.org/10.1063/1.4927470

Mykhailo, C., Ivan, K., Peter, K., Tomáš, D., Valérie, P., Arnaud, C., Nataliya, T., Vladimír, M., & Kateřina, V. (2019). Tailoring of highly porous SnO_2 and SnO_2-Pd thin films. *Materials Chemistry and Physics*, 232, 485-492. https://doi.org/10.1016/j.matchemphys.2018.11.022

Orimi, L. R., & Maghouli, M. (2016). Optical characterization of SnO_2 nanostructure thin films, annealed at different temperatures. *Optik,* 127(1), 263-266. https://doi.org/10.1016/j.ijleo.2015.10.033

Oros, C., Horprathum, M., Wisitsoraat, A., Srichaiyaperk, T., Samransuksamer, B., Limwichean, S., Eiamchai, P., Phokharatkul, D., Nuntawong, N., Chananonnawathorn, C., Patthanasettakul, V., Klamchuen, A., Kaewkhao, J., Tuantranont, A., & Chindaudom, P. (2016). Ultra-sensitive NO_2 sensor based on vertically aligned SnO_2 nanorods deposited by DC reactive magnetron sputtering with glancing angle deposition technique. *Sensors and Actuators B: Chemical*, 223, 936-945. https://doi.org/10.1016/j.snb.2015.09.104

Pan, L., Li, W., Yang, S-E., Zang, J., Guo, H., Xia, T., Shen, W., & Chea, Y. (2019). Effects of annealing conditions on the properties of SnO films deposited by e-beam evaporation process. *Materials Letters,* 257, Article 126737. https://doi.org/10.1016/j.matlet.2019.126737

Patrun, D., Zhao, S., Aytuna, Z., Fischer, T., Miess, M., Hong, Z., & Mathur, S. (2024). Plasma-enhanced SnO_{2-x} thin films on copper current collector for safer lithium metal batteries. *Nano Energy*, 128(Part A), Article 109836. https://doi.org/10.1016/j.nanoen.2024.109836

Rasoo, S., Saritha, K., Reddy, K. T. R., Tivanov, M. S., Gremenok, V. F., Zimin, S. P., Pipkova, A. S., Mazaletskiy, L. A., & Amirov, I. I. (2020). Annealing and plasma treatment effect on structural, morphological and topographical properties of evaporated β-In_2S_3 films. *Materials Research Express,* 7(1), Article 016431. https://doi.org/10.1088/2053-1591/ab6a5b

Song, Y. G., Shim, Y. S., Kim, S., Han, S. D., Moon, H. G., Noh, M. S., Lee, K., Lee, H. R., Kim, J. S., Ju, B. K., & Kang, C. Y. (2017). Downsizing gas sensors based on semiconducting metal oxide: Effects of electrodes on gas sensing properties. *Sensors and Actuators B: Chemical,* 248, 949-956. https://doi.org/10.1016/j.snb.2017.02.035

Sun, C., Yang, J., Xu, M., Cui, Y., Ren, W., Zhang, J., Zhao, H., & Liang, B. (2022). Recent intensification strategies of SnO_2-based photocatalysts: A review. *Chemical Engineering Journal,* 427, Article 131564. https://doi.org/10.1016/j.cej.2021.131564

Tao, Y., Zhu, B., Yang, Y., Wu, J., & Shi, X. (2020). The structural, electrical, and optical properties of SnO_2 films prepared by reactive magnetron sputtering: Influence of substrate temperature and O_2 flow rate. *Materials Chemistry and Physics,* 250, Article 123129. https://doi.org/10.1016/j.matchemphys.2020.123129

Velevska, J., Stojanov, N., Pecovska-Gjorgjevich, M., & Najdoski, M. (2017). Electrochromism in tungsten oxide thin films prepared by chemical bath deposition. *Journal of Electrochemical Science and Engineering*, 7(1), 27-37. https://doi.org/10.5599/jese.357

Xavier, J. R., Dhanalakshimi, C., Chandraraj, S. S., & Vinodhini, S. P. (2023). Bionanocomposites containing SnO_2 with improved chemical resistance and hydrophobic behaviours for applications in food packaging industry, *Transactions of Nonferrous Metals Society of China*, 33(7), 2136-2154. https://doi.org/10.1016/S1003-6326(23)66249-1

Xie, Z., Shuang, S., Ma, L., Zhu, F., Liu, X., & Zhang, Z. (2017). Annealing effect on the photoelectrochemical and photocatalytic performance of TiO_2 nanorod arrays. *RSC Advances,* 7(81)*,* 51382-51390. https://doi.org/10.1039/C7RA09801D

Zakaria, Y., Aïssa, B., Fix, T., Ahzi, S., Samara, A., Mansour, S., & Slaoui, A. (2022). Study of wide bandgap SnO_x thin films grown by a reactive magnetron sputtering via a two-step method. *Scientific Reports*, 12(1), Article 15294. https://doi.org/10.1038/s41598-022-19270-w

Zhang, Y., Li, J., An, G., & He, X. (2010). Highly porous SnO_2 fibers by electrospinning and oxygen plasma etching and its ethanol-sensing properties. *Sensors and Actuators B: Chemical*, 144(1), 43-48. https://doi.org/10.1016/j.snb.2009.10.012